

DFENet: A Novel Dimension Fusion Edge Guided Network for Brain MRI Segmentation

Hritam Basak* · Rukshanda Hussain ·
Ajay Rana

Received: date / Accepted: date

Abstract The rapid increment of morbidity of brain stroke in the last few years have been a driving force towards fast and accurate segmentation of stroke lesions from brain MRI images. With the recent development of deep-learning, computer-aided and segmentation methods of ischemic stroke lesions have been useful for clinicians in early diagnosis and treatment planning. However, most of these methods suffer from inaccurate and unreliable segmentation results because of their inability to capture sufficient contextual features from the MRI volumes. To meet these requirements, 3D convolutional neural networks have been proposed, which, however, suffer from huge computational requirements. To mitigate these problems, we propose a novel Dimension Fusion Edge-guided network (DFENet) that can meet both of these requirements by fusing the features of 2D and 3D CNNs. Unlike other methods, our proposed network uses a parallel partial decoder (PPD) module for aggregating and upsampling selected features, rich in important contextual information. Additionally, we use an edge-guidance and enhanced mixing loss for constantly supervising and improvising the learning process of the network. The proposed method is evaluated on publicly available Anatomical Tracings of Lesions After Stroke (ATLAS) dataset, resulting in mean DSC, IoU, Precision and Recall values of 0.5457, 0.4015, 0.6371, and 0.4969 respectively. The results, when

H. Basak
Department of Electrical Engineering, Jadavpur University, Kolkata, India
E-mail: hritambasak48@gmail.com

R. Hussain
Department of Electrical Engineering, Jadavpur University, Kolkata, India
E-mail: rukhshanda189@gmail.com

A. Rana
Department of Computer Science Engineering, SRM Institute of Science and Technology,
Chennai, India
E-mail: ajay.rana6288@gmail.com

*Corresponding Author: Hritam Basak

compared to other state-of-the-art methods, outperforms them by a significant margin. Therefore, the proposed model is robust, accurate, superior to the existing methods, and can be relied upon for biomedical applications.

Keywords Stroke Lesion Segmentation · MRI · Dimension Fusion · Partial Decoder · Edge Guidance

1 Introduction

Cerebrovascular accident is among the commonest of diseases, prevailing amongst the community in age groups of 40 to 60 contributing to a huge percentage of death worldwide every year [1,2]. Studies have shown that they can even cause disabilities in adults for 2 to 5 years in about 37-71% of reported cases globally. Rehabilitation may be constructive for an eventual recovery in acute conditions with its effectiveness depending on the neurological developments and damages caused by a stroke in the patients. However, significant improvements in neuro-imaging including the brain image analysis and the T1-weighted high-quality MRI images have proven to be contributory for researchers in the diagnosis of patients, improvements in treatment procedures or the likelihood of gaining back some functionality like the motor speech [3]. Brain MRI segmentation is an important task because it influences the entire diagnosis with the processing steps depending on accurate segmentation of various anatomical regions. MRI combined with other diagnostic procedures thus helps in the detection of minor strokes and the presence of Ischemia that may result in Ischemic strokes. In recent days, CNN and DNN models have proven to be remarkably convenient for classification and segmentation purposes [4,5,6,7,8,9,10,13], providing an end-to-end pipeline for segmentation tasks. This is non-identical to the traditional hand-crafted feature extraction and segmentation which were done in problems of classical image processing. The 2-D CNN is used to convert the volumetric data of MRI images into two-dimensional slices, predicting the result. With each iteration, the network improves its result by minimizing these losses. However, as considerable spatio-temporal information is obscured in this approach, the researchers have been shifting towards 3-D CNNs.

3-D CNNs are trained to utilize this crucial information in volumetric data and to segregate and outline any abnormalities in the domain of medical imaging. Nonetheless, the memory and computational requirements used for 3-D CNNs are difficult to meet. Hence, they have been mostly avoided even though they might be useful to extract substantial volumetric information. The U-net architectures have been quite instrumental in present days for the stated purpose [11,12], however, they are unable to extract enough information through 2D operations from 3D MRI data. For solving the problem in segmentation of the areas of stroke-lesion precisely, in this paper we propose a novel dimensionally fused U-net framework which, despite having a 2-D framework, can also associate with relevant spatial 3-D information besides the 2-D information with considerably lower resources as for memory requirements and dataset

are concerned. Besides, instead of generating a segmentation map through the traditional upsampling layers, we propose a parallel partial decoder (PPD) module, that aggregates the features from different layers of the CNN for a better saliency map. It takes in the contextual information to generate a global segmentation map acting as the prediction of the proposed network.

MRI images often contain regions containing a certain level of similarity between two adjacent classes (foreground and background in this case). Hence, accurate prediction of class boundary is somehow difficult for regions having higher-level semantic information from both of the classes. To mitigate this problem, an edge attention module is associated for better representation of the respective edge information of the stroke lesions. Also, we propose an enhanced mixing loss function that combines the standard BCE loss function along with the weighted IoU loss function that helps in enhancing the gradient propagation and achieving faster convergence. As a result of this enhanced deep supervision, the proposed model learns sufficient and important gradient information of pixel intensity and edge information, leading to an accurate and improved segmentation map.

Overview and contribution

This paper proposes a novel segmentation framework that utilizes both 3D and 2D CNN information for accurate segmentation of stroke lesion. The contribution of the paper is described as follows:

1. We propose a novel dimension fusion block to integrate the features from 2D and 3D CNNs for better spatio-temporal feature representation. The proposed model is lightweight as compared to 3D CNNs, providing superior performance than 2D CNNs.
2. Instead of simple upsampling layers, we propose a parallel partial decoder (PPD) module to associate features from deep layers of CNN, containing high-level semantic information for a better saliency map.
3. The shallow features obtained from the first convolution layer of the CNN is used for edge guidance for accurate mapping of image regions near lesion boundary.
4. We propose an enhanced mixing loss function integrating the traditional weighted IoU and BCE loss function for better supervision and faster convergence.

2 Literature Survey

Recent researches in the literature mostly address the problem of lesion segmentation from brain MRI as a semantic segmentation by producing dense pixel-wise predictions for every slice. Quite noteworthy outcomes have been attained by researchers using handcrafted features for brain MRI segmentation purposes in the last few years [32]. However, recent advancements in deep

learning algorithms have inspired researchers to effectively utilize CNN based approach for supervised lesion segmentation. These approaches rely upon deep hierarchical features extracted from volumetric MR data and through a series of convolution operations, produce the final prediction map. However, these methods often suffer from loss of contextual information of fine-grained boundary regions through a series of downsampling and pooling operations in the case of deep CNNs. Secondly, training traditional CNN models requires lots of labelled data which is often not present in brain MRI dataset. These challenges lead to shallow networks with intelligent orientations of layers, that requires fewer parameters and small contextual information for superior performance.

A multivariate CTP based segmentation technique of MRI images with a chance of infarct voxelwise was presented by Kemling et al. [38] whereas Nabizadeh et al. [43] proposed a histogram improvement algorithmic law by using DWI for ischemic lesion segmentation. A multimodal MRI image localization method was then projected by Mitra et al. [44] for the feature mining followed by a Random Forest method for the lesion segmentation which decreased the false positive rate considerably.

UNet [15] is often considered as the state-of-the-art for segmentation of biomedical images, though several modifications have been proposed in recent years to improve the overall learning and feature representation [27, 33, 34, 35, 36, 37]. The input taken by primary convolutional UNet and consequent models is the 2D slices of the MRI image in a solitary orientation. The dual-path CNN, DeepMedic [39], however not considering multiple 2D alignments, have two pathways. The first is for excessive and the other is for low-resolution slices. Lyksborg et al. [40] use a 3-path network, each of the canonical axial, sagittal and coronal views. Formerly [41] eight dissimilar network paths have been discovered for multi-path systems. When supplementing paths, however, arises with a cost of having to suitable many extra parameters for each path [42]. Multi-course structures ought to additionally associate the forecasts from every course right into a closing output. One method to combine path predictions is an easy majority vote. This was the method used by [40]. The intention in their network changed into segmenting tumours, where the pathology may purpose a somewhat dissimilar problem than stroke.

3 Proposed Method

In this section, we explain the workflow of our proposed method, the network architecture, different modules and blocks used, the proposed loss function and the hyperparameters involved.

3.1 Feature Extraction and aggregation

The primary architecture of the proposed network is built upon the U-Net as the base model with a few additional modifications. A UNet-like encoder

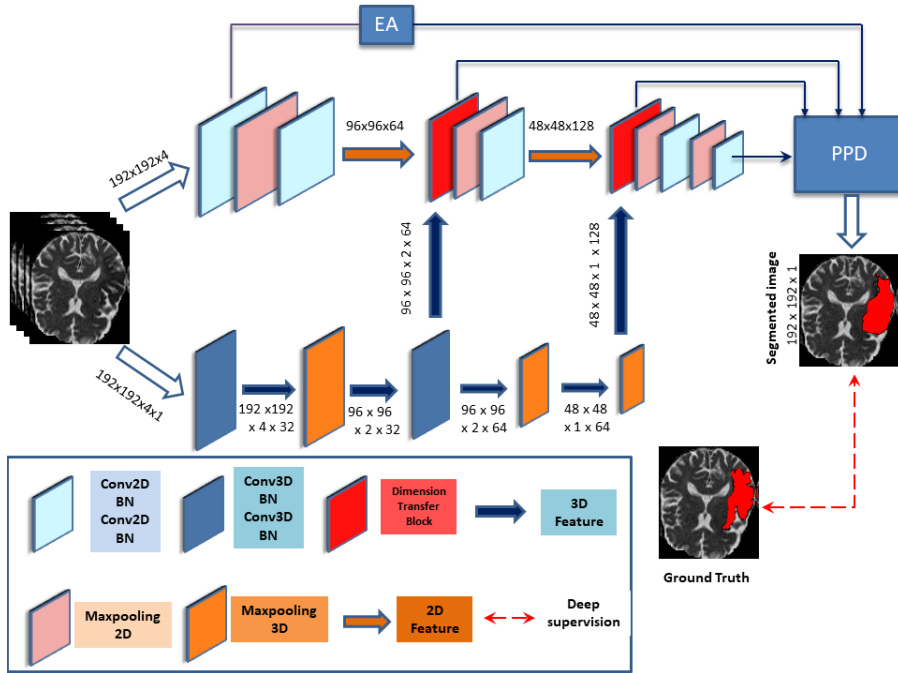


Fig. 1 The overall workflow of the proposed DFENet.

architecture has been developed to extract both high-level semantics and the low-level surface information with the architecture being presented in Figure 1. The depth, width, and height of the considered feature volume are represented by D, W, H whereas the total number of channels present in the obtained feature map is represented by C . The proposed network consists of two parallel branches used for extraction of 2D and 3D spatial information from the volumetric MR dataset, and later merged by using a dimension fusion block, shown in Figure 1. Following the original work of [31], the squeeze and excite (SE) block is being implemented inside the dimension fusion block, consisting of a hyper-parameter called the reduction ratio, represented by r , used to regulate the performance and computational cost, enhancing the fusion effect of two dimensional and three-dimensional features by opening the connection in between these feature channels. These special architectural blocks are utilized for a channel-wise dynamic re-calibration of considered features, hence allowing the network the extraction of essential spatial features.

Every single channel feature is average-pooled into a singular value, following which is a dense layer that is supplemented by employing the ReLU activation. The activation function provides non-linearity and results in a reduction of the output's channel complexity considerably. Finally, the former layer is followed by an additional dense layer as well as a sigmoid such that each channel is receiving a smooth gating function. The 'excitation' part of the SE block is the weighting of every feature map present in the side network but

at a relatively lower computational cost. Thus, even smaller regions of stroke lesions, considered of utmost importance in various applications of medicine, can be easily detected following the given approach.

If F_{2d} and F_{3d} are used to denote the two and three-dimensional feature maps consecutively, which are the inputs for the dimension transfer block, shown in Figure 2, whilst the depth, width, height, the number of channels and the batch size of feature map are represented by D, W, H, C, N respectively. Firstly there is a conversion in the dimension of the F_{3d} from $N \times H \times W \times D \times C$ to $N \times H \times W \times D \times 1$ to produce intermediate feature F_{*3d} which is done with the help of the convolution operation utilizing a 3D $1 \times 1 \times 1$ convolutional block. Following this, there is a reduction in the dimensionality of F_{*3d} from $N \times H \times W \times D \times 1$ to $N \times H \times W \times D$ using squeeze block. However, to maintain the consistency in dimension with the two-dimensional feature maps, the F_{*3d} is converted from having a dimension of $N \times H \times W \times D$ to $N \times H \times W \times C$ by applying a 2D 3×3 convolutional block setting the filter size to C . f_d is used to denote the dimensionality reduction operation function where the conversion of F_{3d} to F'_{3d} is done on application of the stated function (where F'_{3d} is having a dimension of $N \times H \times W \times C$):

$$F'_{3d} = f_d(F_{3d}) \quad (1)$$

$$F_{3d} = f_d(F_{3d}) \quad (2)$$

Next, the SE block is used to aggregate the feature channels of two different dimensions where channel outputs are weighted and thus considered for better proficiency in feature expression before fusion. Mathematically, F (where F is having a dimension of $N \times H \times W \times C$) is denoting a fused feature map that is obtained in the form of an output of the SE block. Further parameters existing in the entire network and its architecture are described in Figure 2. In this step, the features from two different dimensions are fused, where f_s is representing the SE block that squeezes as well as excites, described in [21].

$$F = f_s(F'_{3d}) + f_s(F_{2d}) \quad (3)$$

3.2 Edge Attention

Accurate segmentation of regions near lesion boundary from biomedical images is quite challenging due to the high-level semantic information shared between two adjacent classes (foreground and background) near lesion boundaries. Zhao et al. [14] proposed that fine-grained boundary constraints can provide useful supervision over the feature extraction task for image segmentation, leading to accurate localization of ROI. Later, similar claims were made by Et-Net [15] here the authors utilized edge attention representations in the early encoding stage and later transferred them to multi-stage decoding layers for biomedical image segmentation. Hence, being inspired by the original work

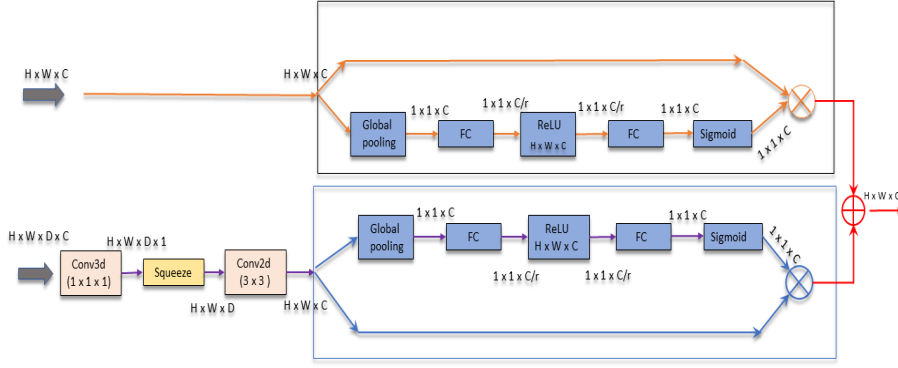


Fig. 2 Architecture of the Dimension transfer block, where the Squeeze and Excite (SE) network is the primary component, marked inside the rectangles, for aggregating 2D and 3D features.

of DANet [16] we introduce a supervised edge attention module to the segmentation framework to effectively learn the edge information from the instances. Here position attention module, as suggested by [16], enhances the representation capability of the local features by aggregating a wide range of contextual information into them. In addition to the original DANet, we add additional convolution layers after the position attention module to obtain edge attention features of the same depth as the feature.

Let $F_A \in \mathbb{R}^{h \times w \times c}$ be a local feature, where h , w , and c represent the height, width and channel respectively, be fed to three convolution layers to produce three new feature maps F_B , F_C and F_D , where $\{F_B, F_C, F_D\} \in \mathbb{R}^{h \times w \times c}$. F_B , F_C and F_D are then reshaped to $n \times c$, where $n = h \times w$ represents the number of pixels. Then F_B is multiplied with transpose of F_C , followed by a *softmax* to obtain edge attention map $\mathcal{M}_E \in \mathbb{R}^{n \times n}$.

$$\mathcal{M}_E(j, i) = \frac{\exp(F_B^i \cdot F_C^j)}{\sum_{i=1}^n \exp(F_B^i \cdot F_C^j)} \quad (4)$$

where $\mathcal{M}_E(j, i)$ represents the impact of the i^{th} position pixel's on that of the j^{th} position's. In parallel, F_D is multiplied with transpose of \mathcal{M}_E and the output is reshaped to $h \times w \times c$. Finally, a multiplication factor β is multiplied to it and the result is element-wise summed up with F_A to produce the final output of EA module O_{EA} , given by the following equation:

$$O_{EA}(j) = \beta \sum_{i=1}^n [F_A(i) + \{F_D(i) \times \mathcal{M}_E(j, i)\}] \quad (5)$$

The output from the EA module is then fed to the PPD block for better edge supervision of the overall segmentation process. The workflow of the EA block is shown in Figure 3.

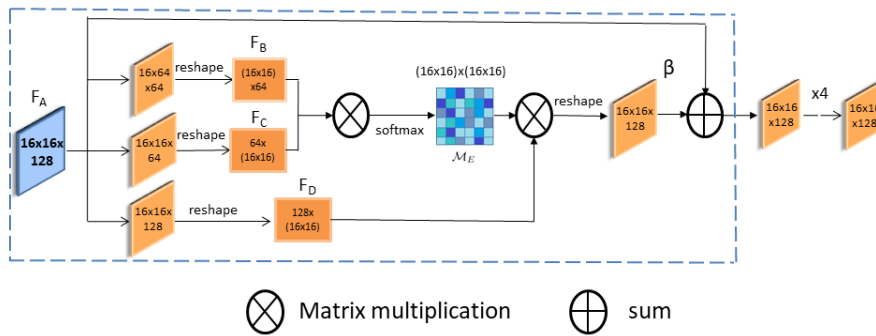


Fig. 3 The workflow of the proposed EA module. The part inside the gridline is inspired by the Position Attention module from DANet [16].

3.3 Parallel Partial Decoder Module

Traditional segmentation models in the U-Net family [17,18] utilizes symmetrical encoder-decoder architecture, providing similar importance to high-level and low-level features to produce the final segmentation map. However, [19] suggested that low-level features contribute very little towards the final prediction map, leading to unnecessary usage of computational resource due to their high spatial resolution. To mitigate this problem, instead of aggregating features from all level of CNN followed by sequential upsampling, we have used a partial decoder module that utilizes inputs from selected CNN layers only. Being inspired by the Receptive Field Block (RFB) [20], our proposed PPD module captures global contextual information to produce an accurate segmentation map.

The initial convolution layers of the CNN are considered the shallow layers and provide information with very little significance towards the final prediction. Hence, they are discarded from the inputs of the PPD module. Specifically, the features from the two-dimension transfer blocks are considered as the major inputs of the PPD module because of their richness in important spatio-temporal information, both in 2D and 3D space. Additionally, the feature from the final downsampling layer and the output from the EA module is also fed to the PPD module. To accelerate the feature propagation, we add a series of convolution and batch normalization operations as shown in Figure 4. Short skip connections are added in the PPD module, similar to the original RFB module. After obtaining different discriminating features from different layers, we finally multiply them to reduce the gap between multiple feature levels. Thus, the PPD module produces a global segmentation map through a series of element-wise multiplication and concatenation operations. The overall architecture of the PPD module is shown in Figure 4.

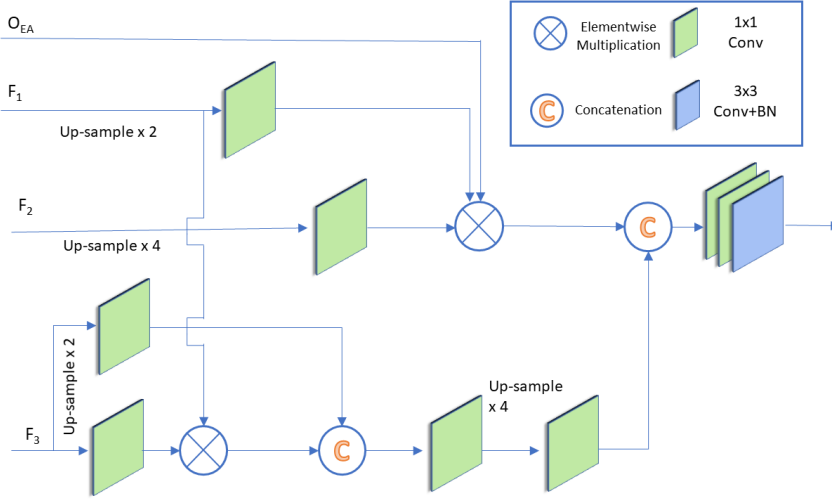


Fig. 4 The proposed Parallel Partial Decoder (PPD) module that utilizes three different feature inputs from different CNN layers and edge attention output to generate the global segmentation map. Here O_{EA} represents output from EA module, F_1 and F_2 represent features from dimension transfer block-1 and 2 respectively, F_3 is the feature from final downsampling block.

3.4 Enhanced Mixing Loss

To supervise the overall learning and segmentation process of the proposed network, we have used an enhanced mixing loss function to mitigate the problems of standard $L1$ and $L2$ loss functions. This hybrid loss function incorporates the features of weighted BCE and weighted IoU loss functions, leading to fast convergence and efficient global and local supervision.

The result from the EA module O_{EA} is supervised with respect to the actual edge map G_E , obtained by calculating the gradient of the ground truth. The standard BCE loss function is used to calculate the dissimilarity between these two as follows:

$$\mathcal{L}_{EA} = - \sum_i G_E \log(O_{EA}) + (1 - G_E) \log(1 - O_{EA}) \quad (6)$$

where i indicates the pixel value of the segmentation map.

The weighted BCE loss function, commonly known as WCE [23], is a modification of standard BCE loss, useful in biomedical application where class imbalance between foreground and background pixel is evident. The formulation of WCE loss in our case is as follows:

$$\mathcal{L}_{WBCE} = - \sum_i \beta \times G \log(O_S) + (1 - G) \log(1 - O_S) \quad (7)$$

where β is the correcting factor, used to tune the false positive and false negative predictions, G is the ground truth, O_S being the prediction map.

Similarly, we calculate the weighted IoU loss function \mathcal{L}_{WIoU} and define the overall loss function \mathcal{L} as:

$$\mathcal{L} = \mathcal{L}_{WIoU}(O_S, G) + \delta \times \mathcal{L}_{WBCE}(O_S, G) + \mathcal{L}_{EA}(O_{EA}, G_E) \quad (8)$$

4 Results and Discussions

In this section, we describe the results obtained, both quantitatively and qualitatively, the experimentations performed, ablation studies and the comparison of our results with those of the state-of-the-art, to evaluate the comparative performance of the proposed method.

4.1 Evaluation metrics

To evaluate the performance of the proposed model on the supervised stroke lesion segmentation task, we have utilized four standard and widely used evaluation metrics, described as follows:

4.1.1 Dice Similarity Coefficient(DSC)

It is a spatial overlap metric that is computed as in Equation 9 for predicted image S and ground truth G .

$$DSC(S, G) = \frac{2 \times |S \cap G|}{|S| + |G|} \quad (9)$$

4.1.2 Intersection over Union (IoU)

Also known as Jaccard Index (JI), it measures the accuracy of segmentation by computing the ratio of the intersection of objects and their union when projected on the same plane. Mathematically it is expressed as in Equation 10, where S is the predicted segmentation mask and G is the original ground truth mask of the image.

$$IoU(S, G) = \frac{|S \cap G|}{|S \cup G|} \quad (10)$$

4.1.3 Precision

It adequately refers to the unadulterated positive detections concerning the actual ground truth. Precision addresses how many of the pixels in the segmentation map matches the verified ground truth observations. Mathematically it is expressed as in Equation 11, where TPs and FPs are the true positive and the false positive respectively.

$$Precision = \frac{TP}{TP + FP} \quad (11)$$

4.1.4 Recall

It effectively expresses, how complete the positive predictions are concerning the actual ground truth. Amongst the total pixels annotated in the verified ground truth, it refers to the number of pixels that were captured as positive predictions. Mathematically it is expressed as in Equation 12, where TP and FN indicate true positive and false negative respectively.

$$Recall = \frac{TP}{TP + FN} \quad (12)$$

4.2 Implementation

The proposed method was implemented in Python, utilizing Nvidia K80 GPU with 12 GB available RAM. An SGD optimizer with reduced learning is utilized where the learning rate is reduced by a factor of 0.1 on the performance metrics plateaus on the validation set, whereas the initial learning rate was set to $1e - 4$. The proposed method was evaluated on Anatomical Tracings of Lesions After Stroke (ATLAS) [24] dataset, consisting of 229 T1 weighted 3D MRI images for stroke lesion segmentation, collected from 11 cohorts worldwide. Each of the images consists of 189 slices, manually segmented by expert practitioners for stroke lesions. The original images have dimensions of 233×197 , resized to 224×192 to remove the unnecessary regions, thereby reducing computations. The reduction factor r of the SE block is set to 16, the batch size is set to 8, maximum iteration is set to 200, early stopping is included.

4.3 Ablation study

To study the importance of different modules of the proposed DFENet, we have performed ablation studies by removing a particular module or part of the architecture, keeping all the other learning parameters and network unchanged. Table 1 shows the experimental analysis of this study, leading to the conclusive decisions of the importance of EA, PPD and SE blocks. These blocks, as shown from the table, when integrated with the base model, has boosted the mean DSC and IoU scores from 0.4606 (UNet) to 0.5481 (proposed) and from 0.3447 (UNet) to 0.4015 (proposed) respectively. It is evident from the table that 2D and 3D UNet can produce not so accurate results on the segmentation dataset, whereas combining the features of the former one with the previous one can boost up the performance (instance 3 in Table 1) by aggregating sufficient contextual and spatio-temporal information, which can not be explored using mere 2D UNet. Replacing the upsampling block of UNet with the proposed PPD can effectively increase the performance by effectively capturing long-range dependencies of the network and discarding the shallow features that contribute less towards the final segmentation output, as shown

Table 1 The results obtained from the ablation studies on the ATLAS dataset to evaluate their importance.

Instances	Combination	Result			
		DSC	IoU	Precision	Recall
1	2D UNet (base model)	0.4606	0.3447	0.5994	0.4449
2	3D UNet (base model)	0.4871	0.3664	0.6027	0.4506
3	2D+3D UNet (using SE)	0.5094	0.3787	0.6061	0.4773
4	2D+3D UNet+PPD	0.5383	0.4029	0.6297	0.4821
5	2D+3D UNet+EA	0.5281	0.4003	0.6139	0.4833
Proposed	2D+3D UNet+EA+PPD	0.5457	0.4015	0.6371	0.4969

in instance 4. The shallow level feature, however, if effectively used through an edge attention module, can also make a significant impact towards the final prediction, as shown in instance 5 of Table 1. The last row depicts the overall performance of the proposed DFENet on the ATLAS dataset.

4.4 Comparison with state-of-the-art

To validate the effectiveness of the proposed DFENet, we have compared our results quantitatively with several other existing methods that have been successfully used for accurate segmentation of stroke lesions on the ATLAS dataset. Table 2 depicts this comparison of our results with UNet [25], SegNet [26], ResUNet [27], PSPNet [28], DeepLab V3 [29], and XNet [30]. To analyze the visual results of the superiority of the proposed method over the existing ones, the visual comparison of some selected segmentation instances are shown in Figure 5. It is evident from the figure that, SegNet often misses important and minor lesion regions (row 1), leading to poor overall performance as shown in Table 2. Though UNet performs quite well in other biomedical segmentation applications and is considered as a state-of-the-art model, it fails to detect sufficient information for accurate lesion segmentation from the ATLAS dataset as compared to the proposed DFENet, shown both in Table 1 and Table 2. XNet and ResUNet on the other hand consistently produced a segmentation map, very close to the proposed DFENet, which is also reflected in Table 2. We can conclude that the proposed DFENet outperforms all the existing methods in this particular segmentation task.

5 Conclusion and Future Works

To gracefully address the shortcomings of existing segmentation methods, in this paper we present an end-to-end segmentation framework for stroke lesion segmentation that can be instrumental in the early detection of cerebrovascular stroke and aid clinicians in treatment planning accordingly. The proposed DFENet can effectively extract information-rich contextual features and can predict accurate segmentation map by fusing 2D and 3D features. The proposed method is robust, effective and when compared to traditional segmenta-

Table 2 Comparison of the quantitative results of the proposed DFENet with several other existing methods on the ATLAS dataset.

Dataset	Method	Result			
		DSC	IoU	Precision	Recall
ATLAS	UNet [25]	0.4606	0.3447	0.5994	0.4449
	SegNet [26]	0.2767	0.1911	0.3938	0.2532
	ResUNet [27]	0.4702	0.3549	0.5941	0.4537
	PSPNet [28]	0.3571	0.2541	0.4769	0.3335
	DeepLab V3 [29]	0.4609	0.3458	0.5831	0.4491
	XNet [30]	0.4867	0.3723	0.6	0.4752
	DFENet (Proposed)	0.5457	0.4015	0.6371	0.4969

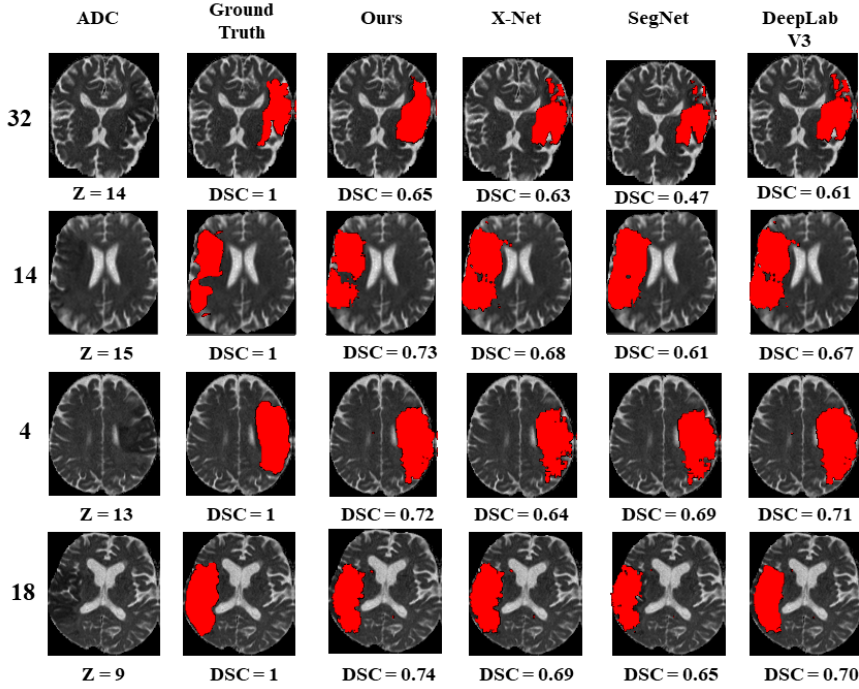


Fig. 5 Visual Comparison of the segmentation results from our proposed method along with different existing methods. The first column represents the original input image of the Apparent Diffusion Coefficient (ADC) MRI sequence in 2D format along with their cut coordinate along x-axis included, the second column is the ground truth, the third column represents the segmentation map from our result. Along with visual comparison, we have also included the DSC scores to identify the accuracy of segmentation.

tion models, outperforms them quite significantly, adding to its reliability and clinical importance. In future, we plan to extend the model for semi-supervised segmentation to address the problem of the insufficient labelled dataset. This paper can be used as a testbed for further experimentations and the development of diverse segmentation frameworks for other biomedical applications as well.

Compliance with Ethical Standards

Funding

The authors did not receive support from any organization for the submitted work. No funding was received to assist with the preparation of this manuscript.

Conflict of Interest

Hritam Basak declares that he has no conflict of interest. Rukshanda Hussain declares that she has no conflict of interest. Ajay Rana declares that he has no conflict of interest.

Ethical Approval

This article does not contain any studies with human participants or animals performed by any of the authors.

References

1. Redon, J., Olsen, M., Cooper, R., Zurriaga, O., Martinez-Beneito, M., Laurent, S., Cifkova, R., Coca, A. and Mancia, G., 2011. Stroke mortality and trends from 1990 to 2006 in 39 countries from Europe and Central Asia: implications for control of high blood pressure. *European Heart Journal*, 32(11), pp.1424-1431.
2. Donkor, E., 2018. Stroke in the 21st Century: A Snapshot of the Burden, Epidemiology, and Quality of Life. *Stroke Research and Treatment*, 2018, pp.1-10.
3. Neumann, A., Jonsdottir, K., Mouridsen, K., Hjort, N., Gyldensted, C., Bizzi, A., Fiehler, J., Gasparotti, R., Gillard, J., Hermier, M., Kucinski, T., Larsson, E., Sørensen, L. and Østergaard, L., 2009. Interrater Agreement for Final Infarct MRI Lesion Delineation. *Stroke*, 40(12), pp.3768-3771.
4. Kamnitsas, K., Ledig, C., Newcombe, V., Simpson, J., Kane, A., Menon, D., Rueckert, D. and Glocker, B., 2017. Efficient multi-scale 3D CNN with fully connected CRF for accurate brain lesion segmentation. *Medical Image Analysis*, 36, pp.61-78.
5. Guerrero, R., Qin, C., Oktay, O., Bowles, C., Chen, L., Joules, R., Wolz, R., Valdés-Hernández, M., Dickie, D., Wardlaw, J. and Rueckert, D., 2018. White matter hyperintensity and stroke lesion segmentation and differentiation using convolutional neural networks. *NeuroImage: Clinical*, 17, pp.918-934.
6. Atlason, H., Love, A., Sigurdsson, S., Gudnason, V. and Ellingsen, L., 2019. SegAE: Unsupervised white matter lesion segmentation from brain MRIs using a CNN autoencoder. *NeuroImage: Clinical*, 24, p.102085.
7. Joshi, S., 2018. Ischemic Stroke Lesion Segmentation by Analyzing MRI Images Using Deep Convolutional Neural Networks. *HELIX*, 8(5), pp.3721-3725.
8. Praveen GB, Agrawal A, Sundaram P, Sardesai S. Ischemic stroke lesion segmentation using stacked sparse autoencoder. *Computers in biology and medicine*. 2018 Aug 1;99:38-52.
9. Liu, L., Chen, S., Zhang, F., Wu, F., Pan, Y. and Wang, J., 2019. Deep convolutional neural network for automatically segmenting acute ischemic stroke lesion in multi-modality MRI. *Neural Computing and Applications*, 32(11), pp.6545-6558.

10. Nazari-Farsani, S., Nyman, M., Karjalainen, T., Bucci, M., Isoj arvi, J. and Nummenmaa, L., 2020. Automated segmentation of acute stroke lesions using a data-driven anomaly detection on diffusion weighted MRI. *Journal of Neuroscience Methods*, 333, p.108575.
11. Y. Weng, T. Zhou, Y. Li and X. Qiu, "NAS-Unet: Neural Architecture Search for Medical Image Segmentation," in *IEEE Access*, vol. 7, pp. 44247-44257, 2019, doi: 10.1109/ACCESS.2019.2908991.
12. Zhang, J., Lv, X., Sun, Q., Zhang, Q., Wei, X. and Liu, B., 2019. SDResU-Net: Separable and Dilated Residual U-Net for MRI Brain Tumor Segmentation. *Current Medical Imaging Formerly Current Medical Imaging Reviews*, 15.
13. Chattopadhyay S, Basak H. Multi-scale Attention U-Net (MsAUNet): A Modified U-Net Architecture for Scene Segmentation. arXiv preprint arXiv:2009.06911. 2020 Sep 15.
14. Zhao JX, Liu JJ, Fan DP, Cao Y, Yang J, Cheng MM. EGNet: Edge guidance network for salient object detection. In *Proceedings of the IEEE/CVF International Conference on Computer Vision 2019* (pp. 8779-8788).
15. Zhang Z, Fu H, Dai H, Shen J, Pang Y, Shao L. Et-net: A generic edge-attention guidance network for medical image segmentation. In *International Conference on Medical Image Computing and Computer-Assisted Intervention 2019 Oct 13* (pp. 442-450). Springer, Cham.
16. Fu J, Liu J, Tian H, Li Y, Bao Y, Fang Z, Lu H. Dual attention network for scene segmentation. In *Proceedings of the IEEE/CVF Conference on Computer Vision and Pattern Recognition 2019* (pp. 3146-3154).
17. Chen W, Liu B, Peng S, Sun J, Qiao X. S3D-UNet: separable 3D U-Net for brain tumor segmentation. In *International MICCAI Brainlesion Workshop 2018 Sep 16* (pp. 358-368). Springer, Cham.
18. Hwang H, Rehman HZ, Lee S. 3D U-Net for skull stripping in brain MRI. *Applied Sciences*. 2019 Jan;9(3):569.
19. Wu Z, Su L, Huang Q. Cascaded partial decoder for fast and accurate salient object detection. In *Proceedings of the IEEE/CVF Conference on Computer Vision and Pattern Recognition 2019* (pp. 3907-3916).
20. Liu S, Huang D. Receptive field block net for accurate and fast object detection. In *Proceedings of the European Conference on Computer Vision (ECCV) 2018* (pp. 385-400).
21. Hu, J., Shen, L. and Sun, G., 2018. Squeeze-and-excitation networks. In *Proceedings of the IEEE conference on computer vision and pattern recognition* (pp.71327141).
22. Lin, T.Y., Goyal, P., Girshick, R., He, K. and Doll ar, P., 2017. Focal loss for dense object detection. In *Proceedings of the IEEE international conference on computer vision* (pp. 2980-2988).
23. Pihur V, Datta S, Datta S. Weighted rank aggregation of cluster validation measures: a monte carlo cross-entropy approach. *Bioinformatics*. 2007 Jul 1;23(13):1607-15.
24. Liew SL, Anglin JM, Banks NW, Sondag M, Ito KL, Kim H, Chan J, Ito J, Jung C, Khoshab N, Lefebvre S. A large, open source dataset of stroke anatomical brain images and manual lesion segmentations. *Scientific data*. 2018 Feb 20;5(1):1-1.
25. Ronneberger O, Fischer P, Brox T. U-net: Convolutional networks for biomedical image segmentation. In *International Conference on Medical image computing and computer-assisted intervention 2015 Oct 5* (pp. 234-241). Springer, Cham.
26. Badrinarayanan V, Kendall A, Cipolla R. Segnet: A deep convolutional encoder-decoder architecture for image segmentation. *IEEE transactions on pattern analysis and machine intelligence*. 2017 Jan 2;39(12):2481-95.
27. Zhang Z, Liu Q, Wang Y. Road extraction by deep residual u-net. *IEEE Geoscience and Remote Sensing Letters*. 2018 Mar 8;15(5):749-53.
28. Zhao H, Shi J, Qi X, Wang X, Jia J. Pyramid scene parsing network. In *Proceedings of the IEEE conference on computer vision and pattern recognition 2017* (pp. 2881-2890).
29. Chen LC, Zhu Y, Papandreou G, Schroff F, Adam H. Encoder-decoder with atrous separable convolution for semantic image segmentation. In *Proceedings of the European conference on computer vision (ECCV) 2018* (pp. 801-818).
30. Qi K, Yang H, Li C, Liu Z, Wang M, Liu Q, Wang S. X-net: Brain stroke lesion segmentation based on depthwise separable convolution and long-range dependencies. In *International Conference on Medical Image Computing and Computer-Assisted Intervention 2019 Oct 13* (pp. 247-255). Springer, Cham.

31. Hu J, Shen L, Sun G. Squeeze-and-excitation networks. In Proceedings of the IEEE conference on computer vision and pattern recognition 2018 (pp. 7132-7141).
32. Shao W, Huang SJ, Liu M, Zhang D. Querying Representative and Informative Super-Pixels for Filament Segmentation in Bioimages. *IEEE/ACM transactions on computational biology and bioinformatics*. 2019 Jan 14;17(4):1394-405.
33. Weng Y, Zhou T, Li Y, Qiu X. NAS-Unet: Neural architecture search for medical image segmentation. *IEEE Access*. 2019 Apr 4;7:44247-57.
34. Basak H., Rana A. F-UNet: A Modified U-Net Architecture for Segmentation of Stroke Lesion. In: Singh S.K., Roy P., Raman B., Nagabhushan P. (eds) *Computer Vision and Image Processing. CVIP 2020. Communications in Computer and Information Science*, vol 1376. Springer, Singapore.
35. Li X, Chen H, Qi X, Dou Q, Fu CW, Heng PA. H-DenseUNet: hybrid densely connected UNet for liver and tumor segmentation from CT volumes. *IEEE transactions on medical imaging*. 2018 Jun 11;37(12):2663-74.
36. Huang H, Lin L, Tong R, Hu H, Zhang Q, Iwamoto Y, Han X, Chen YW, Wu J. Unet 3+: A full-scale connected unet for medical image segmentation. In ICASSP 2020-2020 IEEE International Conference on Acoustics, Speech and Signal Processing (ICASSP) 2020 May 4 (pp. 1055-1059). IEEE.
37. Basak H, Ghosal S, Sarkar M, Das M, Chattopadhyay S. Monocular Depth Estimation Using Encoder-Decoder Architecture and Transfer Learning from Single RGB Image. In 2020 IEEE 7th Uttar Pradesh Section International Conference on Electrical, Electronics and Computer Engineering (UPCON) 2020 Nov 27 (pp. 1-6). IEEE.
38. Kemmling A, Flottmann F, Forkert ND, Minnerup J, Heindel W, Thomalla G, Eckert B, Knauth M, Psychogios M, Langner S, Fiehler J. Multivariate dynamic prediction of ischemic infarction and tissue salvage as a function of time and degree of recanalization. *Journal of Cerebral Blood Flow & Metabolism*. 2015 Sep;35(9):1397-405.
39. Kamnitsas K, Ledig C, Newcombe VF, Simpson JP, Kane AD, Menon DK, Rueckert D, Glocker B. Efficient multi-scale 3D CNN with fully connected CRF for accurate brain lesion segmentation. *Medical image analysis*. 2017 Feb 1;36:61-78.
40. Lyksborg M, Puonti O, Agn M, Larsen R. An ensemble of 2D convolutional neural networks for tumor segmentation. In *Scandinavian Conference on Image Analysis 2015 Jun 15* (pp. 201-211). Springer, Cham.
41. de Brebisson A, Montana G. Deep neural networks for anatomical brain segmentation. In Proceedings of the IEEE conference on computer vision and pattern recognition workshops 2015 (pp. 20-28).
42. Bernal J, Kushibar K, Asfaw DS, Valverde S, Oliver A, Martí R, Lladó X. Deep convolutional neural networks for brain image analysis on magnetic resonance imaging: a review. *Artificial intelligence in medicine*. 2019 Apr 1;95:64-81.
43. Nabizadeh N, Kubat M, John N, Wright C. Automatic ischemic stroke lesion segmentation using single mr modality and gravitational histogram optimization based brain segmentation. In Proceedings of the International Conference on Image Processing, Computer Vision, and Pattern Recognition (IPCV) 2013 (p. 1). The Steering Committee of The World Congress in Computer Science, Computer Engineering and Applied Computing (WorldComp).
44. Mitra J, Bourgeat P, Fripp J, Ghose S, Rose S, Salvado O, Connelly A, Campbell B, Palmer S, Sharma G, Christensen S. Lesion segmentation from multimodal MRI using random forest following ischemic stroke. *NeuroImage*. 2014 Sep 1;98:324-35.